

# Optimal reconstruction of the Hellings and Downs correlation

Bruce Allen\*

Max Planck Institute for Gravitational Physics (Albert Einstein Institute),  
Leibniz Universität Hannover, Callinstraße 38, D-30167, Hannover, Germany

Joseph D. Romano†

Department of Physics and Astronomy, University of Texas Rio Grande Valley,  
One West University Boulevard, Brownsville, TX 78520, USA

(Dated: July 16, 2024)

Pulsar timing arrays (PTAs) detect gravitational waves (GWs) via the correlations they create in the arrival times of pulses from different pulsars. The mean correlation, a function of the angle between the directions to two pulsars, was predicted in 1983 by Hellings and Downs (HD). Observation of this angular pattern is the “smoking gun” that GWs are present, so PTAs “reconstruct the HD curve” by estimating the correlation using pulsar pairs separated by similar angles. Several studies have examined the amount by which this curve is expected to differ from the HD mean. The variance arises because (a) a finite set of pulsars at specific sky locations is used, (b) the GW sources interfere, and (c) the data are contaminated by noise. Here, for a Gaussian ensemble of sources, we predict that variance using an optimal estimator of the HD correlation, taking into account the pulsar sky locations and the power spectrum of the GWs. The variance is a ratio: the numerator depends upon the pulsar sky locations, and the denominator is the number of frequency bins for which the GW signal dominates the noise. In effect, after suitable combination, each frequency bin gives an independent estimate of the HD correlation.

*Introduction.*—As pulsar timing arrays (PTAs) work towards  $5\sigma$  detections of gravitational waves (GWs) [1–4], there is growing interest in different aspects of the underlying physics. This includes potential GW sources, mechanisms that influence pulsar rotation, and the propagation, detection, and analysis of electromagnetic pulses. These, in turn, inform the data analysis.

If GWs had large amplitudes, their effects on the arrival times of pulses from a single pulsar would be directly visible. Early work [5] set upper limits on the GW amplitude using individual pulsars, but it is now known that GW effects are small compared to pulsar timing noise. So, to detect GWs, PTAs search for GW-induced correlations in the arrival times of pulses from *different* pulsars.

The correlation  $-1 \leq \frac{3}{2}\mu \leq 1$  in pulsar timing residuals is a function of the angle  $\gamma \in [0, \pi]$  between the directions to pulsars. These “spatial” or “angular” correlations can be expressed as a sum of Legendre polynomials

$$\mu(\gamma) = \sum_l c_l P_l(\cos \gamma). \quad (1)$$

The coefficients  $c_l$  are estimated from the data: 100 pulsars would give values of  $\mu$  at 4950 angles  $\gamma > 0$ .

The expected pattern of correlation (assuming a stationary, isotropic and unpolarized background) was predicted in 1983 by Hellings and Downs (HD). This function  $\mu_u$  is plotted in the top panel of Fig. 1 and is called the “HD curve” [6]:

$$\begin{aligned} \mu_u(\gamma) &\equiv \langle \mu(\gamma) \rangle = \sum_l \langle c_l \rangle P_l(\cos \gamma) \\ &= \frac{1}{3} + \frac{1 - \cos \gamma}{2} \left[ \ln \left( \frac{1 - \cos \gamma}{2} \right) - \frac{1}{6} \right]. \end{aligned} \quad (2)$$

The expected coefficients  $\langle c_0 \rangle = 0$ ,  $\langle c_1 \rangle = 0$ , and

$$\langle c_l \rangle = (2l + 1)/((l + 2)(l + 1)l(l - 1)) \text{ for } l \geq 2, \quad (3)$$

are computed in [7–9]. (The correlation is doubled to  $3\mu_u(0) = 1$  for pulsars that are closer together than the typical GW wavelength [10, App. C.2].) Detection of the HD curve provides evidence that the pulsar arrival time fluctuations are due to GWs [11].

How closely do we expect that the actual correlations in our (realization of the) Universe will follow this curve? Even if the measurement noise is small, deviations occur because of (1) pulsar variance and (2) cosmic variance. The first arises because observations are carried out with a finite set of pulsars at specific sky locations [12]. The second arises because our Universe has a discrete set of GW sources with specific frequencies, sky locations, and other parameters. Interference between these GW sources means that even if (1) is eliminated by using many pulsars [10, 13, 14], the pulsar-averaged correlation curve [15] will still differ from the HD curve.

We quantify such deviations via the variance

$$\sigma_\mu^2(\gamma) \equiv \langle \mu(\gamma)^2 \rangle - \langle \mu(\gamma) \rangle^2, \quad (4)$$

noting that its value and meaning depend upon the statistical ensemble used for the angle brackets.

*Previous work.*—The topic was first examined by Roebber and Holder [8]. They assumed that the sources form an isotropic and unpolarized Gaussian ensemble radiating GWs at a single frequency, and that noise-free measurements are carried out using an infinite number of pulsars. While not given in this form (see [10, App. C6]

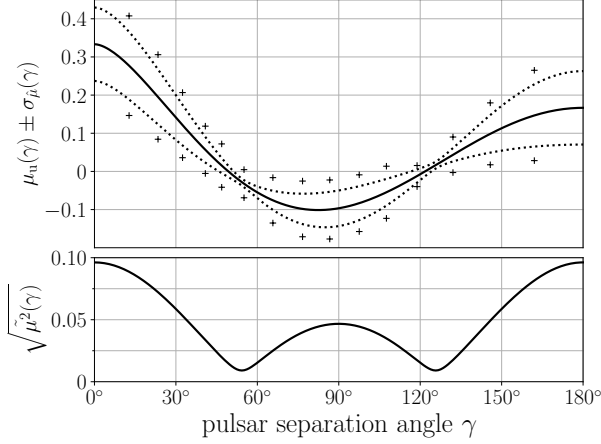


FIG. 1. Top: the black line is the HD curve  $\mu_u(\gamma)$  of (2). The “+” symbols are our predicted  $\pm 1\sigma_u$  deviations for a reconstruction using the 15 angular bins and 66 pulsar sky locations of NANOGrav [2], for  $N_f = 1$ . The dotted line is the same prediction in the limit of an infinite number of pulsars (7). Bottom: square root of the function  $\tilde{\mu}^2(\gamma)$  of (5).

and [16]), they obtain

$$\sigma_\mu^2(\gamma) = \tilde{\mu}^2(\gamma) \equiv \sum_l \frac{\langle c_l \rangle^2}{2l+1} P_l^2(\cos \gamma), \quad (5)$$

whose square root is shown in the bottom panel of Fig. 1. This follows from a sky-map decomposition of the GW background into spherical harmonics  $Y_{lm}(\Omega_p)$  where  $\Omega_p$  is the pulsar location on the two-sphere [9]. For fixed  $l$ , there are  $(2l+1) \times 2$  (GW polarizations) real amplitudes. Each is an independent Gaussian random variable, so the  $c_l$  are  $\chi^2$  distributed with  $k = 4l+2$  degrees of freedom. Since this distribution has mean  $k$  and variance  $2k$ , the ratio of the variance to the squared mean is  $2/k = 1/(2l+1)$  as seen in (5). This variance was also found in [10] [with a closed form for  $\tilde{\mu}^2(\gamma)$ , Eq. (G11)], where it was shown to arise from interference between GW sources.

More recent work examines the effects of pulsar variance and cosmic variance [10]. Using the “pulsar averaging” technique of Cornish and Sesana [15], this shows how to separate pulsar and cosmic variance. These are computed for a Gaussian ensemble with an arbitrary spectrum, and for two different discrete-source ensembles, each containing  $N$  circularly polarized GW sources. If the GW sources radiate at different frequencies and do not interfere, then the cosmic variance vanishes. In contrast, if the sources radiate at the same frequency, then interference produces cosmic variance. In the limit  $N \rightarrow \infty$ , this recovers the Roebber and Holder result, provided that the density of sources approaches infinity with the strength of each source vanishing in a way that keeps the mean-squared strain at Earth constant. These results have also been extended to ensembles containing  $N$  elliptically polarized GW sources, corresponding to circular binaries with randomly oriented orbital planes [17].

These studies compute the cosmic variance for a large number of pulsars, uniformly spread on the sky. Later work shows how to combine measurements from a specific set of pulsars at specific sky locations, to produce a minimum variance estimator of the HD correlation [12]. It proves that the cosmic variance of the Gaussian ensemble is the variance of the optimal estimator of the pulsar-averaged correlation, in the limit of large numbers of uniformly distributed pulsars. It also demonstrates how the transition from pulsar variance to cosmic variance takes place, as more pulsars are added to a PTA.

In all of this previous work, the quantity used to estimate the correlation  $\mu$  was a general linear combination of the “zero-lag” time-averaged product of redshifts

$$\rho_{ab} \equiv \overline{Z_a(t)Z_b(t)} \equiv \frac{1}{T} \int_{-T/2}^{T/2} dt Z_a(t)Z_b(t). \quad (6)$$

Here,  $a, b$  label pulsars,  $Z_a(t)$  is the redshift of pulsar  $a$  at time  $t$  on Earth, and overbar denotes the average over observation time  $T$ . The linear combination of  $\rho_{ab}$  was picked to form an unbiased, minimum variance estimator.

*Summary.*—In this paper, we construct the best possible estimator  $\hat{\mu}$  of the HD correlation for a Gaussian ensemble using a finite set of pulsars. The estimator (23) combines the data in frequency, also incorporating nonzero-lag information. In the limit where there are an infinite number of pulsars, uniformly distributed on the sky, optimally combining the data from different frequencies reduces the cosmic variance to

$$\sigma_{\hat{\mu}}^2 = \frac{1}{N_f} \tilde{\mu}^2(\gamma) \iff \sigma_{\hat{c}_l}^2 = \frac{1}{N_f} \frac{\langle c_l \rangle^2}{2l+1}. \quad (7)$$

Here,  $N_f$  is the number of observational frequency bins in which the GW signal dominates the noise. This generalizes the Roebber and Holder [8]  $N_f = 1$  result (5).

*Derivation.*—In the Earth-pulsar neighborhood, far from any GW sources, GWs are described by a plane-wave expansion [10, Eq. (C1)]. The transverse traceless synchronous metric perturbations arising from GWs are

$$h_{\mu\nu}(t, \mathbf{x}) = \sum_A \int df \int d\Omega h_A(f, \Omega) e_{\mu\nu}^A(\Omega) e^{2\pi i f(t - \mathbf{\Omega} \cdot \mathbf{x})}, \quad (8)$$

where the spatial coordinate  $\mathbf{x} = 0$  at Earth and time  $t$  is measured there. In (8), the GW frequency  $f \in \mathbb{R}$ , the unit vector  $\mathbf{\Omega}$  is the GW propagation direction, touching the unit two-sphere at spherical coordinates  $\Omega = (\theta, \phi)$ . The infinitesimal area on the sphere is  $d\Omega = \sin \theta d\theta d\phi$ , the spatial coordinate indices  $\mu, \nu \in x, y, z$ , the polarization label  $A \in +, \times$ , the polarization tensors  $e_{\mu\nu}^+$  and  $e_{\mu\nu}^\times$  depend upon the GW direction, and  $h_+$  and  $h_\times$  are arbitrary complex functions which satisfy  $h_A^*(f, \Omega) = h_A(-f, \Omega)$ , ensuring that  $h_{\mu\nu}$  is real.

Consider a pulsar  $a$  at distance  $L_a > 0$  from Earth in direction  $\mathbf{\Omega}_a$ , so  $\mathbf{x}_a = L_a \mathbf{\Omega}_a$ . The redshift of the pulsar’s

frequency arising from the GW (8) is

$$Z_a(t) = \sum_A \int df \int d\Omega h_A(f, \Omega) F_a^A(\Omega) \tau(f, L_a \Omega_a, \Omega) e^{2\pi i f t}, \quad (9)$$

where  $t$  is time at Earth. The pulsar “antenna pattern” for polarization  $A$  is

$$F_a^A(\Omega) = \frac{1}{2} \frac{\Omega_a^\mu \Omega_a^\nu e_{\mu\nu}^A(\Omega)}{1 + \Omega \cdot \Omega_a}, \quad (10)$$

with the Einstein summation convention applying to  $\mu$  and  $\nu$ . The factor  $\tau$  forms the difference between Earth and pulsar terms:

$$\tau(f, L_a \Omega_a, \Omega) = 1 - e^{-2\pi i f L_a (1 + \Omega \cdot \Omega_a)}. \quad (11)$$

Expressions (8) and (9) describe the GWs and the redshift over intervals (millions of years) much shorter than the Hubble time; PTAs observe a snapshot of the redshift (9) over a time interval  $T$  of order decades.

Assume that the redshift is observed over a time period  $t \in [-T/2, T/2]$ . Standard observational methods represent this as a Fourier sum

$$Z_a(t) = \sum_j Z_a^j e^{2\pi i f_j t} \text{ for } t \in [-T/2, T/2], \quad (12)$$

where the frequencies  $f_j \equiv j/T$  are integer multiples of  $1/T$ . The sum has  $j \in -N_b, \dots, -1, 1, \dots, N_b$ , where  $N_b$  is the number of frequency bins. For quantities that carry both pulsar and frequency indices, we put pulsar indices  $a, b, c, d, e, f$  down and frequency indices  $j, k, \ell, m$  up.

Multiplying (9) by  $T^{-1} e^{-2\pi i f_k t}$  and integrating over  $t \in [-T/2, T/2]$ , then doing the same to (12) gives the redshift amplitude in the  $k$ 'th frequency bin:

$$Z_a^k = \sum_A \int df \int d\Omega h_A(f, \Omega) F_a^A(\Omega) \times \tau(f, L_a \Omega_a, \Omega) \text{sinc}(\pi(f - f_k)T), \quad (13)$$

where  $\text{sinc } x \equiv (\sin x)/x$ . Since (12) is real,  $Z_a^{k*} = Z_a^{-k}$ . The rhs's of (12) and (13) discard observational noise terms, for reasons that we will discuss later.

Since the parameters (sky positions, distances, frequencies, amplitudes, etc.) of the GW sources contributing to (8) are unknown, we cannot determine the waveforms  $h_A(f, \Omega)$  and predict the redshifts. Instead, we provide a statistical description, assuming that the GWs arise from an incoherent sum of many weak sources, so that the central limit theorem applies.

Let  $h_A(f, \Omega)$  be a representative function drawn from a stationary Gaussian ensemble describing an isotropic and unpolarized background. Using angle brackets to denote averages over this ensemble, the Gaussian process is fully defined by its first  $\langle h_A(f, \Omega) \rangle = 0$  and second moment

$$\langle h_A(f, \Omega) h_{A'}^*(f', \Omega') \rangle = \delta_{AA'} \delta(f - f') \delta^2(\Omega, \Omega') H(f), \quad (14)$$

where  $H(f) = H(-f) \geq 0$  is a real spectrum (see [10, Eqns.(C5-7)] for its relation to the GW power spectrum and other measures of intensity). Higher moments can be computed from the first and second moments via Isserlis's theorem [18].

Since the Fourier coefficients  $Z_a^k$  are linear combinations of the  $h_A(f, \Omega)$ , they are also Gaussian random variables. Their first moments  $\langle Z_a^k \rangle = 0$ , and from (13) and (14) their second moments are

$$\langle Z_a^j Z_b^{k*} \rangle = H_{jk} \mu_{ab}. \quad (15)$$

Here,  $\mathbf{H} \equiv H_{jk}$  is a real bisymmetric  $2N_b \times 2N_b$  matrix

$$H_{jk} \equiv 4\pi \int df H(f) \text{sinc}(\pi(f - f_j)T) \text{sinc}(\pi(f - f_k)T), \quad (16)$$

with rows/columns indexed by frequency bin. It has non-negative eigenvalues, and its matrix inverse is denoted  $\mathbf{H}^{-1}$ ; if  $\det \mathbf{H} = 0$ , then  $\mathbf{H}^{-1}$  denotes the Moore-Penrose pseudoinverse. Since  $H_{jk} = H_{kj} = H_{-k, -j}$ , both  $\mathbf{H}$  and  $\mathbf{H}^{-1}$  are reflection invariant across *either* diagonal.

The object  $\mu \equiv \mu_{ab}$  that appears in (15) is

$$\mu_{ab} \equiv \mu_u(\gamma_{ab})(1 + \delta_{ab}). \quad (17)$$

It has indices labeled by pulsars  $a$  and  $b$ , and its entries are the values of the HD curve at angle  $\gamma_{ab}$ , doubled if  $a$  and  $b$  are the same. The angle  $\gamma_{ab} \in [0, \pi]$  between the lines of sight to  $a$  and  $b$  is defined by  $\cos \gamma_{ab} = \Omega_a \cdot \Omega_b$ .

To obtain (15) and (17), we used the definition of the Hellings and Downs curve

$$\mu_u(\gamma_{ab}) \equiv \frac{1}{4\pi} \sum_A \int d\Omega F_a^A(\Omega) F_b^A(\Omega), \quad (18)$$

and the reasoning given in [10, App. C2] to replace

$$\tau(f, L_a \Omega_a, \Omega) \tau^*(f, L_b \Omega_b, \Omega) \rightarrow 1 + \delta_{ab} \quad (19)$$

within integrals over frequency  $f$  and direction  $\Omega$ .

Later, we will make use of the covariance

$$\begin{aligned} C_{ab,cd}^{jk,\ell m} &\equiv \langle Z_a^j Z_b^k Z_c^{\ell*} Z_d^{m*} \rangle - \langle Z_a^j Z_b^k \rangle \langle Z_c^{\ell*} Z_d^{m*} \rangle \\ &= \langle Z_a^j Z_c^{\ell*} \rangle \langle Z_b^k Z_d^{m*} \rangle + \langle Z_a^j Z_d^{m*} \rangle \langle Z_b^k Z_c^{\ell*} \rangle \quad (20) \\ &= \mu_{ac} \mu_{bd} H_{j\ell} H_{km} + \mu_{ad} \mu_{bc} H_{jm} H_{k\ell}, \end{aligned}$$

where the second equality follows from Isserlis's theorem [18], and the third from (15). (Noise terms, given in [12, Sec. 9], are dropped from (20) for reasons that we will discuss later.) The part of  $C_{ab,cd}^{jk,\ell m}$  which is symmetric in  $jk$  and/or  $\ell m$  is

$$C_{ab,cd}^{(jk),\ell m} = C_{ab,cd}^{jk,(\ell m)} = C_{ab,cd} H_{j(\ell} H_{m)k}. \quad (21)$$

The round brackets denote symmetrization, for example  $Q_{(jk)} \equiv (Q_{jk} + Q_{kj})/2$ . The pulsar-dependent part of the covariance plays an important role in [12], and is

$$C \equiv C_{ab,cd} \equiv \mu_{ac} \mu_{bd} + \mu_{ad} \mu_{bc}. \quad (22)$$

The factorization (21) into a pulsar-dependent term and a frequency-dependent term simplifies what follows.

To estimate the HD correlation at angle  $\gamma$ , we use  $N_{\text{pair}}$  pulsar pairs  $ab$  lying in an angular bin around  $\gamma$ . Following [12], we use  $ab \in \gamma$  to denote this set of pulsar pairs; autocorrelations are excluded, so  $a < b$ . The estimator  $\hat{\mu}$  is a general linear combination

$$\hat{\mu} \equiv \sum_{ab \in \gamma} \sum_{jk} W_{ab}^{jk} Z_a^j Z_b^k \quad (23)$$

of redshift cross-products. The weights  $\mathbf{W} \equiv W_{ab}^{jk}$  are set by requiring that  $\hat{\mu}$  (i) is unbiased, (ii) minimizes the variance among universes drawn from the Gaussian ensemble, and (iii) is real, so  $W_{ab}^{jk*} = W_{ab}^{-j,-k}$ . As mentioned, this is more general than the estimator of [12], which is a linear combination of the zero-lag correlations (6)

$$\rho_{ab} \equiv \overline{Z_a(t) Z_b(t)} = \sum_j Z_a^j Z_b^{j*}, \quad (24)$$

where the final equality follows from substituting (12) into (6). Those estimators have frequency-independent weights  $W_{ab}^{jk}$ , which vanish off the antidiagonal  $j = -k$ . The more general form (23) allows us to further reduce the variance, thus improving the estimator.

Typically, PTA signals and noise follow power laws in frequency. Below some frequency  $f < N_f/T$ , the GW signal dominates the noise, whereas for frequencies  $f > N_f/T$ , the noise dominates. The effect of the noise terms, dropped from (13) and (20), is to cut off the summation over  $jk$  in (23): they cause the weights  $\mathbf{W}$  to fall off [19] if  $|j| > N_f$  or  $|k| > N_f$ . So, from this point forward, summations over frequency indices  $j, k, \ell, m$  are restricted to the range  $-N_f, \dots, -1, 1, \dots, N_f$ , where the GW signal dominates the noise, or equivalently,  $N_b \rightarrow N_f$ .

The optimal weights  $W_{ab}^{jk}$  are found as in [12, Sec. 3A]. From (16), the ensemble average of the estimator (23) is

$$\langle \hat{\mu} \rangle = \sum_{ab \in \gamma} \sum_{jk} \mu_{ab} W_{ab}^{jk} H_{j,-k} = \mu_u(\gamma). \quad (25)$$

This is normalized to  $\mu_u(\gamma)$  to ensure that  $\hat{\mu}$  is unbiased. Because  $H_{j,-k} = H_{-j,k} = H_{k,-j}$  is symmetric in  $jk$ , (25) does not constrain the antisymmetric part of  $W_{ab}^{jk}$ . So, we set those entries to zero, implying  $W_{ab}^{jk} = W_{ab}^{kj} = W_{ab}^{(jk)}$ .

The variance (4) of the estimator  $\hat{\mu}$  is

$$\begin{aligned} \sigma_{\hat{\mu}}^2 &\equiv \langle |\hat{\mu}|^2 \rangle - \langle \hat{\mu} \rangle^2 \\ &= \sum_{ab \in \gamma} \sum_{cd \in \gamma} \sum_{jk} \sum_{\ell m} W_{ab}^{jk} C_{ab,cd}^{jk,\ell m} W_{cd}^{\ell m*} \\ &= \sum_{ab \in \gamma} \sum_{cd \in \gamma} \sum_{jk} \sum_{\ell m} W_{ab}^{jk} C_{ab,cd} H_{j\ell} H_{mk} W_{cd}^{\ell m*}. \end{aligned} \quad (26)$$

The second equality follows from (20) and (23), and the third from (21), since  $W_{ab}^{jk}$  is symmetric in  $jk$ .

It is helpful to introduce an inner product between weights  $\mathbf{A} \equiv A_{ab}^{jk}$  and  $\mathbf{B} \equiv B_{cd}^{\ell m}$ , defined by

$$(\mathbf{A}, \mathbf{B}) \equiv \sum_{ab \in \gamma} \sum_{cd \in \gamma} \sum_{jk} \sum_{\ell m} A_{ab}^{jk} C_{ab,cd} H_{j(\ell} H_{m)k} B_{cd}^{\ell m*}. \quad (27)$$

This is positive definite for weights which are symmetric in the frequency indices, provided that the pulsar positions are generic and that  $H$  has nonzero eigenvalues.

It is also helpful to introduce a set of real weights

$$\mathbf{V} \equiv V_{ab}^{jk} \equiv H_{j,-k}^{-1} \sum_{cd \in \gamma} C_{ab,cd}^{-1} \mu_{cd}. \quad (28)$$

These are symmetric in  $jk$  and satisfy  $V_{ab}^{jk*} = V_{ab}^{-j,-k}$ . Here, the object  $C_{ab,cd}^{-1}$  (see [12]) is defined by

$$\sum_{ef \in \gamma} C_{ab,ef} C_{ef,cd}^{-1} = \delta_{ac} \delta_{bd} + \delta_{ad} \delta_{bc}. \quad (29)$$

We use  $\mathbf{C}$  to denote the  $N_{\text{pair}} \times N_{\text{pair}}$  matrix  $C_{ab,cd}$ , whose rows and columns are labeled by pulsar pairs  $ab \in \gamma$  and  $cd \in \gamma$ ; the object  $C_{ab,cd}^{-1}$  is the matrix inverse  $\mathbf{C}^{-1}$ .

To find the weights  $\mathbf{W}$  that define the minimum-variance estimator  $\hat{\mu}$ , use the inner product (27) to write

$$\langle \hat{\mu} \rangle = (\mathbf{W}, \mathbf{V}) \quad \text{and} \quad \sigma_{\hat{\mu}}^2 = (\mathbf{W}, \mathbf{W}). \quad (30)$$

The first equality requires a few lines of algebra; the second is by inspection. Minimizing the variance subject to the normalization constraint  $\langle \hat{\mu} \rangle = \mu_u(\gamma)$  is equivalent to minimizing the ratio  $(\mathbf{W}, \mathbf{W}) / (\mathbf{W}, \mathbf{V})^2$ . This implies that  $\mathbf{W}$  is proportional to  $\mathbf{V}$ , so  $\mathbf{W} = \mu_u(\gamma) \mathbf{V} / (\mathbf{V}, \mathbf{V})$ . From (27), (28), and (29), the inner product  $(\mathbf{V}, \mathbf{V})$  is

$$(\mathbf{V}, \mathbf{V}) = 2N_f \sum_{ab \in \gamma} \sum_{cd \in \gamma} \mu_{ab} C_{ab,cd}^{-1} \mu_{cd} \equiv 2N_f \boldsymbol{\mu}^t \mathbf{C}^{-1} \boldsymbol{\mu}. \quad (31)$$

[Here, if  $\det \mathbf{H} = 0$ , then  $2N_f$  is replaced by  $\text{rank}(\mathbf{H})$ .] The column vector  $\boldsymbol{\mu}$  has dimension  $N_{\text{pair}}$  and contains values of the HD curve evaluated at the separations of the pulsar pairs in the angular bin.

The variance of the estimator  $\hat{\mu}$  follows from (30):

$$\sigma_{\hat{\mu}}^2 = (\mathbf{W}, \mathbf{W}) = \frac{\mu_u^2(\gamma)}{(\mathbf{V}, \mathbf{V})} = \frac{\mu_u^2(\gamma)}{2N_f \boldsymbol{\mu}^t \mathbf{C}^{-1} \boldsymbol{\mu}}. \quad (32)$$

This is our main result: it is similar to the variance found in [12], but decreases as  $N_f$ , the number of signal-dominated frequency bins, increases. It is independent of the form of the data (e.g., timing residuals or redshifts), because the powers of  $f$  relating them cancel in the product of  $\mathbf{H}$  and  $\mathbf{H}^{-1}$ .

If the angular bin is narrow, then  $\boldsymbol{\mu} \approx \mu_u(\gamma) \mathbf{1}$ , where  $\mathbf{1} = (1, \dots, 1)^t$  is a column vector containing  $N_{\text{pair}}$  ones. For this narrow angular bin, discrete pulsar pair case

$$\sigma_{\hat{\mu}}^2 = (2N_f \mathbf{1}^t \mathbf{C}^{-1} \mathbf{1})^{-1}. \quad (33)$$

If there are many pulsar pairs in a bin at angle  $\gamma$ , uniformly distributed on the sky, then [12] shows that  $(\mathbb{1}^t \mathbf{C}^{-1} \mathbb{1})^{-1} \rightarrow 2\tilde{\mu}^2(\gamma)$ . The variance of  $\hat{\mu}$  then approaches

$$\sigma_{\hat{\mu}}^2 = \frac{1}{N_f} \tilde{\mu}^2(\gamma), \quad (34)$$

which is our other key result (7).

*Conclusion.*— Roebber and Holder [8, end of Sec. 4] write that “separate frequency bins can be considered as independent realizations of the same map”. The word “considered” is needed: since  $\mathbf{H}$  is nondiagonal, the maps are correlated and not independent. This is generic to PTAs, whose observational timespans are much shorter than the coherence time of their GW sources.

Our calculation proves that this (diagonal  $\mathbf{H}$ ) intuition is correct: each signal-dominated frequency bin provides an independent estimator of the HD correlation. Optimally combining the data from these bins thus reduces the total variance in proportion to the number of bins.

It is satisfying that this result also holds for finite numbers of pulsars at specific sky locations, not just in the infinite-pulsar limit, and applies to both timing residuals and redshifts. It holds equally for the variances of  $\mu(\gamma)$  or for its harmonic coefficients  $c_l$  in (1).

Bayesian reconstruction of the HD correlation, starting from PTA data, produces posterior probability distributions for  $\mu(\gamma)$  and  $c_l$ . Because it makes optimal use of all available information, given sensible choices of priors, we expect that the corresponding variances should be in reasonable agreement with our frequentist predictions. This can be tested with (and used to characterize) simulations such as [20].

---

\* bruce.allen@aei.mpg.de

† joseph.romano@utrgv.edu

- [1] J. Antoniadis *et al.* (EPTA and InPTA Collaborations), The second data release from the European Pulsar Timing Array: III. Search for gravitational wave signals, *Astronomy & Astrophysics* **678**, A50 (2023).
- [2] G. Agazie *et al.* (NANOGrav Collaboration), The NANOGrav 15 yr Data Set: Evidence for a Gravitational-wave Background, *The Astrophysical Journal Letters* **951**, L8 (2023).
- [3] D. J. Reardon *et al.* (PPTA Collaboration), Search for an Isotropic Gravitational-wave Background with the Parkes Pulsar Timing Array, *The Astrophysical Journal Letters* **951**, L6 (2023).
- [4] H. Xu *et al.* (CPTA Collaboration), Searching for the Nano-Hertz Stochastic Gravitational Wave Background with the Chinese Pulsar Timing Array Data Release

I, *Research in Astronomy and Astrophysics* **23**, 075024 (2023).

- [5] V. M. Kaspi, J. H. Taylor, and M. F. Ryba, High-Precision Timing of Millisecond Pulsars. III. Long-Term Monitoring of PSRs B1855+09 and B1937+21, *Astrophys. J.* **428**, 713 (1994).
- [6] R. W. Hellings and G. S. Downs, Upper limits on the isotropic gravitational radiation background from pulsar timing analysis, *Astrophys. J.* **265**, L39 (1983).
- [7] J. Gair, J. D. Romano, S. Taylor, and C. M. F. Mingarelli, Mapping gravitational-wave backgrounds using methods from CMB analysis: Application to pulsar timing arrays, *Phys. Rev. D* **90**, 082001 (2014).
- [8] E. Roebber and G. Holder, Harmonic space analysis of pulsar timing array redshift maps, *Astrophys. J.* **835**, 21 (2017).
- [9] B. Allen, Pulsar timing array harmonic analysis and source angular correlations, arXiv:2404.05677 (2024), to appear in PRD, arXiv:2404.05677 [gr-qc].
- [10] B. Allen, Variance of the Hellings-Downs correlation, *PRD* **107**, 043018 (2023).
- [11] B. Allen, S. Dhurandhar, Y. Gupta, M. McLaughlin, P. Natarajan, R. M. Shannon, E. Thrane, and A. Vecchio, The International Pulsar Timing Array checklist for the detection of nanoHertz gravitational waves (2023), arXiv:2304.04767 [astro-ph.IM].
- [12] B. Allen and J. D. Romano, Hellings and Downs correlation of an arbitrary set of pulsars, *Phys. Rev. D* **108**, 043026 (2023).
- [13] J. D. Romano and B. Allen, Answers to frequently asked questions about the pulsar timing array Hellings and Downs curve (2024), to appear in CQG, arXiv:2308.05847 [gr-qc].
- [14] B. Allen, Will pulsar timing arrays observe the Hellings and Downs correlation curve?, in *18th Vulcano Workshop: Frontier Objects in Astrophysics and Particle Physics*, Vol. 74, edited by A. Antonelli, R. Fusco Femiano, A. Morselli, and G. C. Trinchero (2022) pp. 65–80.
- [15] N. J. Cornish and A. Sesana, Pulsar timing array analysis for black hole backgrounds, *Classical and Quantum Gravity* **30**, 224005 (2013).
- [16] R. C. Bernardo and K.-W. Ng, Pulsar and cosmic variances of pulsar timing-array correlation measurements of the stochastic gravitational wave background, *J. C. A. P.* **2022**, 046 (2022).
- [17] B. Allen and S. Valtolina, Pulsar timing array source ensembles, *Phys. Rev. D* **109**, 083038 (2024).
- [18] L. Isserlis, On a formula for the product-moment coefficient of any order of a normal frequency distribution in any number of variables, *Biometrika* **12**, 134 (1918), often called “Wick’s Theorem” by physicists, although Wick’s work was three decades later.
- [19] B. Allen and J. D. Romano, Detecting a stochastic background of gravitational radiation: Signal processing strategies and sensitivities, *Phys. Rev. D* **59**, 102001 (1999).
- [20] B. Bécsy, N. J. Cornish, and L. Z. Kelley, Exploring realistic nanoHertz gravitational-wave backgrounds, *The Astrophysical Journal* **941**, 119 (2022).